Molecular Biology of the Cell
Vol. 19, 4521–4533, October 2008

Glial Fibrillary Acidic Protein Filaments Can Tolerate the Incorporation of Assembly-compromised GFAP-δ, but with Consequences for Filament Organization and αB-Crystallin Association

Ming-Der Perng,* Shu-Fang Wen,* Terry Gibbon,* Jinte Middeldorp,† Jacqueline Sluijs,† Elly M. Hol,† and Roy A. Quinlan*

*School of Biological and Biomedical Sciences, The University of Durham, Durham DH1 3LE, United Kingdom; and †Netherlands Institute for Neuroscience, an Institute of the Royal Netherlands Academy of Arts and Sciences, 1105 BA Amsterdam, The Netherlands

Submitted March 14, 2008; Revised July 8, 2008; Accepted July 30, 2008
Monitoring Editor: Thomas D. Pollard

The glial fibrillary acidic protein (GFAP) gene is alternatively spliced to give GFAP-α, the most abundant isoform, and seven other differentially expressed transcripts including GFAP-δ. GFAP-δ has an altered C-terminal domain that renders it incapable of self-assembly in vitro. When titrated with GFAP-α, assembly was restored providing GFAP-δ levels were kept low (~10%). In a range of immortalized and transformed astrocyte derived cell lines and human spinal cord, we show that GFAP-δ is naturally part of the endogenous intermediate filaments, although levels were low (~10%). This suggests that GFAP filaments can naturally accommodate a small proportion of assembly-compromised partners. Indeed, two other assembly-compromised GFAP constructs, namely enhanced green fluorescent protein (eGFP)-tagged GFAP and the Alexander disease–causing GFAP mutant, R416W GFAP both showed similar in vitro assembly characteristics to GFAP-δ and could also be incorporated into endogenous filament networks in transfected cells, providing expression levels were kept low. Another common feature was the increased association of αB-crystallin with the intermediate filament fraction of transfected cells. These studies suggest that the major physiological role of the assembly-compromised GFAP-δ splice variant is as a modulator of the GFAP filament surface, effecting changes in both protein– and filament–filament associations as well as Jnk phosphorylation.

INTRODUCTION

Intermediate filaments (IFs) represent one of the three major cytoskeletal systems found in most eukaryotic cells. There are now 65 different genes in the human genome identified as members of the IF protein family (Oshima, 2007), which are usually expressed in a cell-type specific pattern. They form extensive networks that maintain mechanical strength and shape of the cell and provide dynamic platforms for the organization of the cytoplasm on a structural and functional level (Coulombe and Wong, 2004; Herrmann *et al.*, 2007). The formation of IF networks in cells usually involves more than one IF protein, even for those which can self-assemble in vitro. So for instance, vimentin is found frequently as a heteropolymer with, for example, either desmin (Quinlan and Franke, 1982), glial fibrillary acidic protein (GFAP; Quinlan and Franke, 1983), or nestin (Steinert *et al.*, 1999).

The picture emerging from a large number of studies suggests that every cell type has a distinct IF composition. This can be well demonstrated in astrocytes, in which GFAP, nestin, synemin, and vimentin are the major IF proteins. Vimentin and nestin are mainly expressed in immature astrocytes, whereas vimentin is coexpressed with GFAP in the mature astrocytes (Eliasson *et al.*, 1999). Up-regulation of both GFAP and vimentin and re-expression of nestin are hallmarks of reactive astrocytes in many neuropathologies (Pekny and Pekna, 2004).

The study of mice with targeted deletion of GFAP and/or vimentin (Gomi *et al.*, 1995; Pekny *et al.*, 1995, 1999; McCall *et al.*, 1996) have shown astrocyte IFs to be fundamentally important to the maintenance of CNS homeostasis (Pekny, 2001). Specifically, GFAP is involved in astrocyte volume regulation (Ding *et al.*, 1998), glial scar formation (Pekny *et al.*, 1999), and anchoring glutamate transporters to the plasma membrane to facilitate neurotransmitter recycling (Sullivan *et al.*, 2007). In addition, mice deficient in GFAP and vimentin exhibit improved posttraumatic regeneration of neuronal synapses (Wilhelmsson *et al.*, 2004) and integration of neural grafts (Kinouchi *et al.*, 2003). Moreover, mutations in GFAP cause Alexander disease (Brenner *et al.*, 2001), in which cytoskeletal defects leading to astrocyte dysfunction could have widespread effects on the other cell types of the CNS (Mignot *et al.*, 2004).

The human GFAP gene comprises nine exons spaced over 10 kb on chromosome 17q21 (Reeves *et al.*, 1989; Brenner *et al.*, 1990), and this gene structure is conserved in mouse (Lewis *et al.*, 1984; Balcarek and Cowan, 1985) and rat (Condorelli *et al.*, 1994). Although most IF genes are not alternatively spliced, the GFAP gene is known to generate several

This article was published online ahead of print in *MBC in Press* (http://www.molbiolcell.org/cgi/doi/10.1091/mbc.E08–03–0284) on August 13, 2008.

Address correspondence to: Roy A. Quinlan (r.a.quinlan@durham.ac.uk).

splice variants (for review, see Quinlan *et al.*, 2007 and references therein). One of these is produced by alternative splicing that replaces the last two exons of the most common GFAP isoform GFAP-α gene (Reeves *et al.*, 1989; Bongcam-Rudloff *et al.*, 1991) with an alternative exon located within intron 7. This alternative spliced form was first identified in rat and named as GFAP-δ (Condorelli *et al.*, 1999). The human homologue was named GFAP-ε (Nielsen *et al.*, 2002), but now that the relationship with the rat splice variant is clear, we refer to this splice variant as GFAP-δ. The new exon substitutes the C-terminal tail sequence of 42 residues in GFAP-α with a novel 41-amino acid replacement, to create GFAP-δ.

Although the C-terminal tail of GFAP-α is involved in filament formation and stability (Quinlan *et al.*, 1989; Chen and Liem, 1994), the contribution of the C-terminal tail of GFAP-δ to IF assembly and function remains poorly understood. We show that GFAP-δ is a natural component of filament networks in a range of astrocytoma cell lines and in normal human spinal cord using isoform-specific antisera and yet GFAP-δ is incapable of forming filaments in vitro. The transient overexpression of GFAP-δ resulted in the formation of cytoplasmic aggregates that often collapsed the endogenous GFAP networks, an observation also made for other assembly-compromised GFAP variants, such as the enhanced green fluorescent protein (eGFP)-tagged GFAP and the Alexander disease–causing mutant, GFAP-R416W. This suggests that GFAP filaments have an innate ability to accept and incorporate assembly-compromised GFAP subunits. We demonstrate that the incorporation of GFAP-δ has potentially important functional consequences by increasing the levels of αB-crystallin, a protein chaperone associated with the GFAP filaments, and causing filament aggregation when GFAP-δ levels are increased by transient transfection. Collectively, our findings suggest assembly-compromised GFAP-δ could function to alter protein–protein interactions of GFAP filaments.

MATERIALS AND METHODS

Plasmid Construction

Expression plasmids encoding full-length human GFAP-α were constructed as previously described (Perng *et al.*, 2006). The unique tail domain of GFAP-δ was amplified from human brain cDNA by PCR using oligonucleotides 5′-ATTCCCGTGCAGACCTTCTCCAACCTG-3′ and 5′-GAACGCCGCCGGCTCGCGGTTAGGAATTC-3′ as forward and reverse primers, respectively. The amplified PCR product was purified and cloned into pGEM-Teasy (Promega, Southampton, United Kingdom) vector, and the sequence was confirmed against the GenBank data base entry for the GFAP-δ exon 7a (accession no. AJ306447). For expression in bacteria, GFAP-δ in pGEM-T easy vector was digested with BsgI and EcoRI restriction enzymes to generate a 170-base pair fragment that was then substituted for the corresponding GFAP-α segment in the pET23b vector. An eGFP-tagged GFAP (eGFP-GFAP) construct was made by fusing eGFP to the N-terminus of human GFAP-α cDNA. A HindIII-BamHI fragment containing the human GFAP-α sequence was ligated in-frame into the HindIII and BamHI sites of eGFP-C3 vector (Clontech Laboratories, Palo Alto, CA). The eGFP-GFAP cDNA was then subcloned into pET23d vector using the NcoI and BamHI restriction sites.

Expression and Purification of GFAP-α and GFAP-δ

For bacterial expression of proteins, pET23b vector containing either GFAP-α or -δ or eGFP-GFAP cDNAs were transformed into *Escherichia coli* BL21(DE3) pLysS strain. After transformation, cultures were grown in Luria Bertani medium supplemented with appropriate antibiotics to OD_{600} of 0.5–0.6, and protein expression was induced by the addition of 1 mM isopropyl-1-thio-b-D-galactopyranoside (IPTG) for 4 h. Overexpression of GFAPs formed inclusion bodies, which were prepared as previously described (Quinlan *et al.*, 1989). The final pellet enriched in GFAP was solubilized in extraction buffer (8 M urea, 20 mM Tris-HCl, pH 7.4, 5 mM EDTA, 1 mM EGTA, 1 mM DTT, and 1 mM phenylmethylsulfonyl fluoride [PMSF]) and purified as described elsewhere (Perng *et al.*, 2006). Column fractions were analyzed by SDS-PAGE, and those containing purified GFAP were collected and stored at −80°C. Protein concentrations were determined by bicinchoninic acid assay (BCA reagent, Perbio Science, Chester, United Kingdom) using bovine serum albumin as standard. Recombinant human αB-crystallin was purified as described previously (Perng *et al.*, 1999b).

In Vitro Assembly and Sedimentation Assay

In vitro assembly and sedimentation assays were carried out as described previously (Perng *et al.*, 2006). In brief, purified GFAP was diluted to 0.3 mg/ml in 6 M urea in a low ionic strength buffer (10 mM Tris-HCl, pH 8.0, 5 mM EDTA, 1 mM EGTA, and 1 mM DTT). GFAP samples were dialyzed stepwise against 3 M urea in the same buffer for 4 h and then against the same buffer without urea overnight at 4°C. Filament assembly was completed by dialyzing against assembly buffer (20 mM imidazole, pH 6.8, 100 mM NaCl, and 1 mM DTT) for 12–16 h at room temperature. The efficiency of in vitro assembly was assessed by high-speed sedimentation assay as described elsewhere (Nicholl and Quinlan, 1994). In brief, the assembly mixture was layered onto a 0.85 M sucrose cushion in assembly buffer and was centrifuged at 80,000 × *g* for 30 min. To investigate the extent of filament–filament interactions, assembled filaments were subjected to low-speed centrifugation at 3000 × *g* for 10 min in a Bench Top centrifuge (Eppendorf, Hamburg, Germany). The supernatant and pellet fractions were separated by 12% (wt/vol) SDS-PAGE and visualized by Coomassie Blue staining. The amount of protein in the supernatant and pellet fractions was analyzed by a luminescent image analyzer (LAS-1000plus, FujiFilm, Tokyo, Japan) and quantified using the Image Gauge software (version 4.0, FujiFilm).

In some assays, GFAP-α and -δ were mixed with recombinant human αB-crystallin in low-ionic strength buffer at the indicated molar ratios. Assembly of the GFAP filaments was initiated by addition of a 20-fold concentrated assembly buffer to give a final concentration of 100 mM imidazole-HCl, pH 6.8, 1 mM DTT, and 0.2 mM PMSF. After a 1-h incubation at 37°C, protein samples were subjected to high-speed centrifugation assay, and the supernatant and pellet fractions were compared by SDS-PAGE as described above.

Electron Microscopy

GFAP diluted in assembly buffer to 100 μg/ml was negatively stained with 1% (wt/vol) uranyl acetate (Agar Scientific, Sanstead, United Kingdom). Samples were spread on carbon-coated copper grids and examined with an Hitachi H-7600 transmission electron microscope (Hitachi High-Technologies, Tokyo, Japan), using an accelerating voltage of 100 kV. Images were acquired using a CCD camera (Advanced Microscopy Techniques, Danvers, MA) before being further processed in Adobe Photoshop CS (Adobe Systems, San Jose, CA).

Cell Cultures and Transient Transfection

Established human astrocytoma cell lines (U87G and U373MG) were obtained from the European Collection of Cell Cultures (Sigma, Poole, United Kingdom). The human astrocytoma cell line, U343MG was a gift from Dr. James T. Rutka (Toronto, ON, Canada), and cells were grown in α-MEM (Invitrogen, Paisley, United Kingdom) supplement with 10% (vol/vol) fetal calf serum, 100 U/ml penicillin, 100 μg/ml streptomycin, and 2 mM L-glutamine. Immortalized human astrocytes (Im cells) were a generous gift from Dr. James E. Goldman (Columbia University, New York). Unless otherwise stated, cells were grown in DMEM supplemented with 10% (vol/vol) fetal calf serum, 2 mM L-glutamine, 100 U/ml penicillin, and 100 μg/ml streptomycin (Sigma) and maintained at 37°C in a humidified incubator with 95% (vol/vol) air and 5% (vol/vol) CO_2.

For transient transfection studies, eGFP-GFAP and GFAP-α and -δ in pET23b vector were subcloned into a mammalian expression vector pcDNA3.1(−) (Invitrogen) using XbaI and EcoRI restriction sites. Cells grown on 13-mm coverslips at a density of 40–50% confluency were transfected with pcDNA 3.1(−) vector containing either GFAP-α, GFAP-δ, eGFP-GFAP, or R416W GFAP (Perng *et al.*, 2006) using GeneJuice transfection reagent (Novagen, Nottingham, United Kingdom) according to the manufacturer's protocol. Cells were allowed to recover for 48 h before further processing for double-label immunofluorescence microscopy.

Generation of Stable, Inducible Cell Lines

The U343 Tet-Off cells with tetracycline-repressor gene expression system were maintained in α-MEM growth medium containing 500 μg/ml G418 (Melford Laboratories, Suffolk, United Kingdom). The response vector pTRE2hyg (BD Biosciences, Palo Alto, CA) contains a multiple cloning site immediately downstream of the tetracycline (Tet) response element (TRE) and the minimal CMV promotor. To construct inducible R416W GFAP expression vector, R416W GFAP in pcDNA3.1(−) was subcloned into the pTRE2hyg vector using the NheI and EcoRV restriction sites. The resulting pTRE2hyg-R416WGFAP vector was transfected into the U343 Tet-Off cells using GeneJuice transfection reagent (Novagen). Selection of stable cell lines was initiated 3 d after transfection using 200 μg/ml hygromycin B (Duchefa Biochemie, Haarlem, The Netherlands). Fourteen days after selection, colonies were isolated and cultured in 24-well plates and then transferred into 12- and 6-well plates and finally into 10-cm^2 Petri dishes (Greiner Bio-One,

Stonehouse, Gloucestershire, United Kingdom). The stable cell line (U343-GFAP^{R416W}) was cultivated in growth medium supplemented with 2 μg/ml doxycycline. Expression of R416W GFAP was induced by thoroughly washing the cells with phosphate-buffered saline (PBS) followed by adding fresh medium without doxycycline. The growth medium was changed on the following day to remove the doxycycline completely.

Immunofluorescence Microscopy

Cells grown on coverslips were washed twice with PBS and fixed in ice-cold methanol/acetone (1:1 vol/vol) for 20 min. In the case of transfection with eGFP-GFAP, cells were fixed with 4% (wt/vol) paraformaldehyde in PBS for 10 min and then permeabilized with 0.5% (vol/vol) NP-40 in PBS for 10 min. After washing twice with PBS containing 0.02% (wt/vol) sodium azide and 0.02% (wt/vol) bovine serum albumin (PBS/BSA/azide), cells were blocked with 10% (vol/vol) goat serum in PBS/BSA/azide for 20 min and then incubated with primary antibodies at room temperature for 1 h. The following primary antibodies used in this study were mouse monoclonal anti-human GFAP (SMI-21, 1:500, Sternberger Monoclonals, Baltimore, MD), mouse monoclonal anti-R416W GFAP (1A2, 1:1000; Perng *et al.*, 2006), mouse monoclonal anti-αB-crystallin (2D2B6, 1:1; Sawada *et al.*, 1993), rabbit polyclonal GFAP antibodies (3270, 1:200; Perng *et al.*, 1999a), rabbit polyclonal GFAP-δ antibodies (1:500; Roelofs *et al.*, 2005), and rabbit monoclonal phospho-JNK antibodies (1:100, Cell Signaling Technologies, Beverly, MA). After cells were washed with PBS/BSA/azide, the primary antibodies were detected using Alexa 488 (1:400; Molecular Probes, Eugene, OR) or Alexa 594 (1:600; Molecular Probes)-conjugated secondary antibodies. All antibodies were diluted in PBS/BSA/azide buffer. After staining, the glass coverslips were mounted on slides with the fluorescent protecting agent Citifluor (Citifluor Labs, Birmingham, United Kingdom). Images were acquired using a Zeiss LSM 510 confocal laser scanning microscope (Carl Zeiss, Jena, Germany) with optical sections set to ~1.0 μm. Images were processed and prepared for figures using Adobe Photoshop CS.

Preparation of Cell Lysates and Subsequent Immunoblotting Analyses

To determine the expression levels of the endogenous GFAP-α and -δ, cells grown on 75-cm^2 flasks to 90% confluency were washed with cold PBS and then lysed on ice in extraction buffer (20 mM Tris-HCl, pH 7.4, 5 mM EDTA, 5 mM $MgCl_2$, 140 mM NaCl containing 1% [wt/vol] NP-40 and 0.5% [wt/vol] sodium deoxycholate supplemented with Complete protease inhibitor cocktail; Roche Diagnostics, Mannheim, Germany; and 1 mM PMSF) containing 250 U/ml benzonase nuclease (Novagen). Cell lysates were then homogenized in a 1 ml Dounce homogenizer (Wheaton, Millville, NJ). After concentration determination, total cell lysates were equalized by adding appropriate volumes of Laemmli's sample buffer (Laemmli, 1970) before analysis by SDS-PAGE and immunoblotting. To prepare supernatant and pellet fractions, total cell lysates were centrifuged at 16,000 $\times$ *g* for 15 min at 4°C. The resulting pellets were resuspended in Laemmli's sample buffer in a volume that was equivalent to the supernatant. To give an IF-enriched cytoskeletal fraction, the pellet was extracted further with high-salt buffer (20 mM Tris-HCl, pH 7.4, 5 mM EDTA, 140 mM NaCl, 1% [wt/vol] Triton X-100, and 1.5 M KCl). In some experiments, cells were subjected to a mild extraction protocol using a lysis buffer as described previously (Perng *et al.*, 2006).

Immunoblotting was performed using the semidry blotting method according to the manufacturer's specifications (Bio-Rad Laboratories, Hemel Hempstead, Herts, United Kingdom) and modified as described (Perng *et al.*, 2006). Primary antibodies used were mouse monoclonal anti-human GFAP (SMI-21, 1:5000), anti-actin (AC-40, 1:2000, Sigma), anti-αB-crystallin (2D2B6, 1:50; Sawada *et al.*, 1993), anti-HSP27 (heat-shock protein; ERD5, 1:1000; King *et al.*, 1987), rabbit polyclonal anti-GFAP-δ (1:1000; Roelofs *et al.*, 2005), and rabbit monoclonal phospho-JNK antibodies (1:100, Cell Signaling Technologies) antibodies diluted in blocking buffer. In some experiments, a mouse monoclonal anti-GFAP-α antibody (clone-52, BD Biosciences) raised against the C-terminal 15 amino acids of human GFAP was used to specifically detect the GFAP-α. Antibody labeling was detected by enhanced chemiluminescence (ECL plus, Amersham Biosciences, Bucks, United Kingdom) with use of a luminescent image analyzer (LAS-1000plus, FujiFilm). The strength of signal was quantified using the Image Gauge software (Version 4.0, FujiFilm).

qPCR Determination of GFAP-α and -δ mRNA Levels in U343MG Cells

Relative levels of mRNA for the two splice variants GFAP-α and -δ were determined as described (Roelofs *et al.*, 2005). In short, RNA was isolated with Trizol according to the manufacturer and treated with DNase I to prevent contamination with genomic DNA. 2 μg of RNA was reverse-transcribed with Superscript II using hexamer primers, and the cDNA was amplified with primers directed against the 3′ untranslated region (UTR) of GFAP-α and the 3′UTR of GFAP-δ. The GFAP-α primers 388/389 (5′-CTTCTCCAACCTGCAGATTCG-3′ and 5′-CACGGTCTTCACCACGATGTT-3′) also amplify GFAPΔ 164, GFAPΔ exon and GFAPΔ 135, but not GFAP-δ and -κ. The GFAP-δ primers 390/391 (5′-CCGTGCAGACCTTCTCCAA-3′ and 5′-CGTATTGTGAGGCTTTTGAGATATCT-3′) only recognize GFAP-δ and not GFAP-κ. The GFAPΔ 135 primers 992/984 (5′-TCTGCGCGGCACGGAGTA-3′ and 5′-GGGAATGGTGATCCGGTTCT-3′) are isoform specific. The Q-PCR was carried out with the SYBR green PCR kit (Applied Biosystems, Foster City, CA) on an ABI 7300 system. The absolute amounts of GFAP-α and -δ molecules was calculated by comparing the signal of endogenous GFAPs to the signal of a dilution series (10^6, 10^5, 10^4, and 10^4 molecules per PCR reaction) of pcDNA3 plasmid DNA containing either the GFAP-α, the GFAP-δ, or the GFAPΔ 135 sequence. The signal for GFAP-α was corrected for the presence of the GFAPΔ 135 isoform. The data were analyzed with the Sequence Detection Software of Applied Biosystems. The data presented represent the mean from three independent samples.

Human Autopsy Samples

Spinal cord samples (nonneurological control NBB 05-083, 97-156, 99-046, and 99-111) were obtained from the Netherlands Brain Bank, Amsterdam. Spinal cord GFAP was purified by a modification of axonal floating method as described previously (Ralton *et al.*, 1994). Fifteen grams of the frozen spinal cord was ground to powder with a mortar and pestle. Four volumes of cold 0.85 M sucrose in 10 mM Na_2PO_4, pH 7.4, 5 mM EDTA, 0.1 M NaCl, 1% (vol/vol) Triton X-100, 0.2 mM PMSF was added, and the powder was homogenized with a Dounce homogenizer. After 6 h of mixing at 4°C, the homogenate was centrifuged (SW-32 rotor, Beckman Instruments, Fullerton, CA) at 25,000 rpm at 4°C for 30 min. The supernatant was stored at −20°C, and the pellet was homogenized using an Ultraturrax (IKA-Werke, Staufen, Germany) in 20 ml cold 10 mM Na_2PO_4, pH 7.4, 5 mM EDTA, 1.5 M KCl, 0.5% (vol/vol) Triton X-100, 0.2 mM PMSF. This was followed by overnight mixing at 4°C. The homogenate was centrifuged at 18,000 rpm in a SW-32 rotor (ultracentrifuge, Beckman Instruments) for 30 min. The supernatant was discarded, and the pellet was washed in 10 ml cold 10 mM Tris-HCl, pH 7.4, 100 mM NaCl, and 5 mM EDTA. The pellet was stored at −80°C.

The levels of GFAP-α and -δ were analyzed by immunoblotting with antibodies to GFAP-α and -δ. The amounts of GFAP-α and -δ were quantified using the Image Gauge software as described above. Three independent measurements were made per sample to determine the mean value of GFAP-α and -δ levels.

RESULTS

Effect of GFAP-δ upon In Vitro Assembly of GFAP-α

In vitro assembly characteristics of the GFAP isoform, GFAP-δ, were determined. Purified recombinant GFAP-α and -δ were assembled in vitro and analyzed by electron microscopy after negatively staining the samples. Although GFAP-α assembled into typical 10-nm filaments (Figure 1A), this was not the case for GFAP-δ, which failed to form filaments (Figure 1E). Instead, it formed aggregates (Figure 1E) that comprised filamentous-like material (Figure 1E, inset). The GFAP-δ is a minor GFAP isoform (Nielsen *et al.*, 2002), and therefore it is important to consider its assembly in the context of an excess of GFAP-α. When GFAP-δ and -α were coassembled in a 1:19 ratio (i.e., 5% of the total GFAP), the filaments formed were not dramatically altered in morphology (Figure 1B) compared with those made from 100% GFAP-α (Figure 1A). Increasing the proportion of GFAP-δ to 10% in the assembly mixture resulted in filaments that had a marked tendency to aggregate (Figure 1C). At a 1:1 ratio of GFAP-δ, the normal assembly of GFAP-α was disrupted (Figure 1D), and protein aggregates similar to those formed by GFAP-δ alone (Figure 1E) were formed.

We used a low-speed centrifugation assay to monitor the extent of filament aggregation (Perng *et al.*, 2004, 2006). For GFAP-α, approximately a quarter (28%) of the assembled protein was sedimented into the pellet fraction under low-speed centrifugation conditions (Figure 1F, lanes 1 and 2). A high-speed sedimentation assay confirmed that GFAP-α had assembled efficiently, because >95% of the protein was sedimented (data not shown). In contrast, nearly all of the GFAP-δ (>90%) was found in the pellet fraction after low-speed centrifugation when assembled on its own (Figure 1F, lanes 9 and 10). Increasing the proportion of GFAP-δ in mixtures with GFAP-α markedly increased the proportion of GFAP that could be pelleted under low-speed centrifuga-

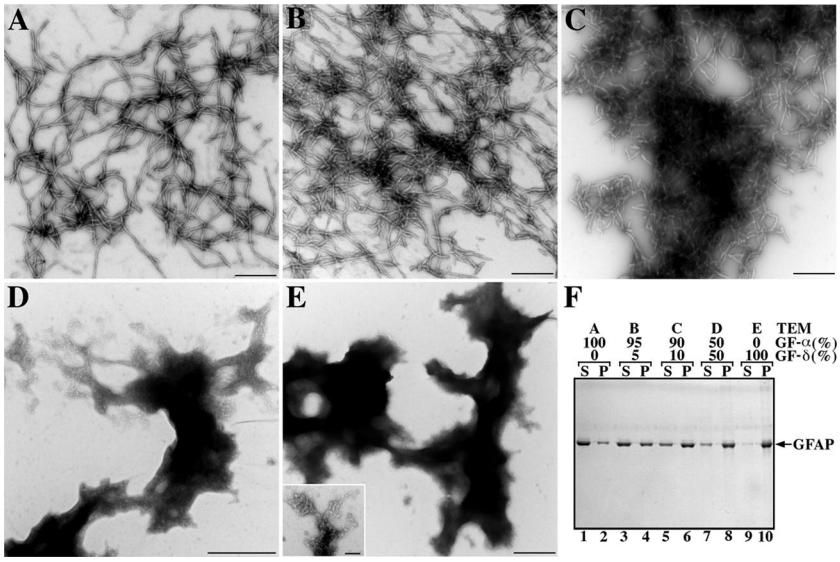

Figure 1. Effects of GFAP-δ upon the in vitro assembly of GFAP-α. Purified GFAP-α and -δ at a concentration of 0.3 mg/ml was assembled in vitro. Assembled filaments were negatively stained and were visualized by transmission electron microscopy. Ten-nanometer-diameter filaments with several micrometers in length are seen for GFAP-α (A). In contrast, GFAP-δ formed irregular structures (E, inset) that had a strong tendency to aggregate (E). Mixing GFAP-δ and -α in 5:95 ratio did not dramatically alter the filament structures formed (B), but increasing the amount of GFAP-δ to 10% resulted in filament aggregation (C). When GFAP-δ was coassembled with GFAP-α in a 50:50 ratio (D), aggregates similar to those formed by GFAP-δ alone (E) were observed. The extent of this aggregation was assessed by a low-speed sedimentation assay (F). The GFAP-α (lanes 1 and 2) and GFAP-δ (lanes 9 and 10) were assembled either individually or in ratios of 95:5 (lanes 3 and 4), 90:10 (lanes 5 and 6), or 50:50 (lanes 7 and 8) ratios of GFAP-α:-δ. After assembly, samples were subjected to low-speed centrifugation, and the resulting supernatant (S) and pellet (P) fractions were analyzed by SDS-PAGE and visualized by Coomassie Blue staining. Increasing the proportion of GFAP-δ in the assembly mixtures dramatically increased GFAP in the pellet fractions (lanes 4, 6, and 8), suggesting GFAP-δ acts dominantly to promote GFAP-α aggregation. Bar, 0.5 μm, except in inset of E, where it is 0.1 μm.

tion conditions (Figure 1F, lanes 4, 6, and 8), suggesting that the presence of GFAP-δ promotes filament aggregation.

Detection of Endogenous GFAP-δ Expression in Human Spinal Cord and Astrocytoma Cell Lines with GFAP-δ Isoform-specific Antibodies

The unique C-terminal tail of GFAP-δ has allowed a polyclonal antibody to be raised against the last 14 amino acids (Roelofs *et al.*, 2005), and the specificity of this antibody was confirmed by immunoblotting of purified recombinant proteins, complimenting the GFAP-α specific mAb, clone 52. Although this GFAP-α–specific mAb recognized predominantly GFAP-α (Figure 2A, lane 1), the anti-GFAP-δ antibody specifically recognized the GFAP-δ (Figure 2A, lane 2). The mAb SMI-21, however, recognizes both GFAP-α and -δ, indicating that the epitope for this antibody resides in the head or rod domain or in the first amino acids of the tail domain.

These GFAP isoform–specific antibodies allowed us to determine the relative expression levels of GFAP-α and -δ in five different samples of human spinal cord (Figure 2, A–G) and also show the distribution of GFAP-δ by immunofluorescence microscopy (Figure 2, H–J). In three of the samples, however, GFAP was so heavily proteolyzed that it compromised the accurate measurement of the GFAP-α-to-GFAP-δ ratio. Analysis of both supernatant and pellet fractions by immunoblotting of the two remaining samples revealed that both GFAP-α and -δ were present almost entirely in the pellet fraction, as illustrated in the example shown (Figure 2, B and C, lanes 1 and 2). A small fraction of GFAP-α remained in the supernatant fraction (data not shown). The amount of GFAP-δ relative to GFAP-α in the pellet fraction was estimated using known amounts of purified recombinant human GFAP-α and -δ as standards (Figure 2, B and C, lanes 3–7). The average level of GFAP-δ was measured to be 8.4 ± 1.27% of the GFAP-α (Figure 2, D–G). Immunofluorescence microscopy (Figure 2, H–J) revealed the signal for GFAP-δ to be concentrated in astrocyte-rich regions of the spinal cord, and the signal at higher magnification is consistent with localization to astrocytic processes and cell bodies (Figure 2, I and J). These findings led us to further investigate the GFAP-α and -δ expression levels in immortalized human astrocytes (Im cells) and a range of astrocytoma-derived cell lines, including U87MG, U373MG, and U343MG cells. The endogenous expression of GFAP-α and -δ were barely detectable in both the immortalized (Im) human astrocytes (Figure 3A, lane 1) and in U87MG astrocytoma cells (Figure 3A, lane 2). In contrast, both U373MG (Figure 3A, lane 3) and U343MG (Figure 3A, lane 4) cells expressed high levels of GFAP-α and detectable levels of GFAP-δ. The relative GFAP-δ to -α level was determined by immunoblotting (Supplementary Figure S1). GFAP-δ was expressed at 14.35 ± 1.07% and 10.13 ± 1.53% of GFAP-α levels in U373MG and U343MG cells, respectively. We also investigated whether protein levels corresponded to mRNAs in U343MG cells. The GFAP-α:GFAP-δ ratio was measured to be 7.96 ± 2.73 in this cell line, suggesting a reasonable correlation between mRNA abundance and protein expression. Both data sets show that GFAP-δ represents only a small fraction of the total GFAP, which is consistent with previous observations (Nielsen *et al.*, 2002; Roelofs *et al.*, 2005).

This GFAP-δ-specific antibody also allowed us to visualize the distribution of the GFAP-δ in human astrocytoma-derived cell lines that have well-established GFAP networks. Both U343MG and U373MG cells were used, but only those data for U343MG cells are presented (Figure 3B-D) as similar results were obtained for U373MG cells (data not shown). The distribution of endogenous GFAP-δ in relation to the GFAP networks was visualized by double-label immunofluorescence microscopy with use of a standard monoclonal anti-human GFAP antibody (SMI-21) and a polyclonal anti-GFAP-δ antibody. The endogenous GFAP-δ (Figure 3B) appeared to localize alone with the GFAP networks (Figure 3, C and D) in U343MG cells, but its presence did not cause collapse of the GFAP networks. When transiently overexpressed in U343 cells, however, GFAP-δ formed cytoplasmic aggregates (Figure 4A) that also disrupted endogenous GFAP networks (Figure 4B). In contrast, cell transfected with GFAP-α mainly formed extended filament networks (Figure 4D, arrows). The relative expression levels and solubility of GFAP-α and -δ were determined by immunoblotting of extracts from U343MG cells prepared

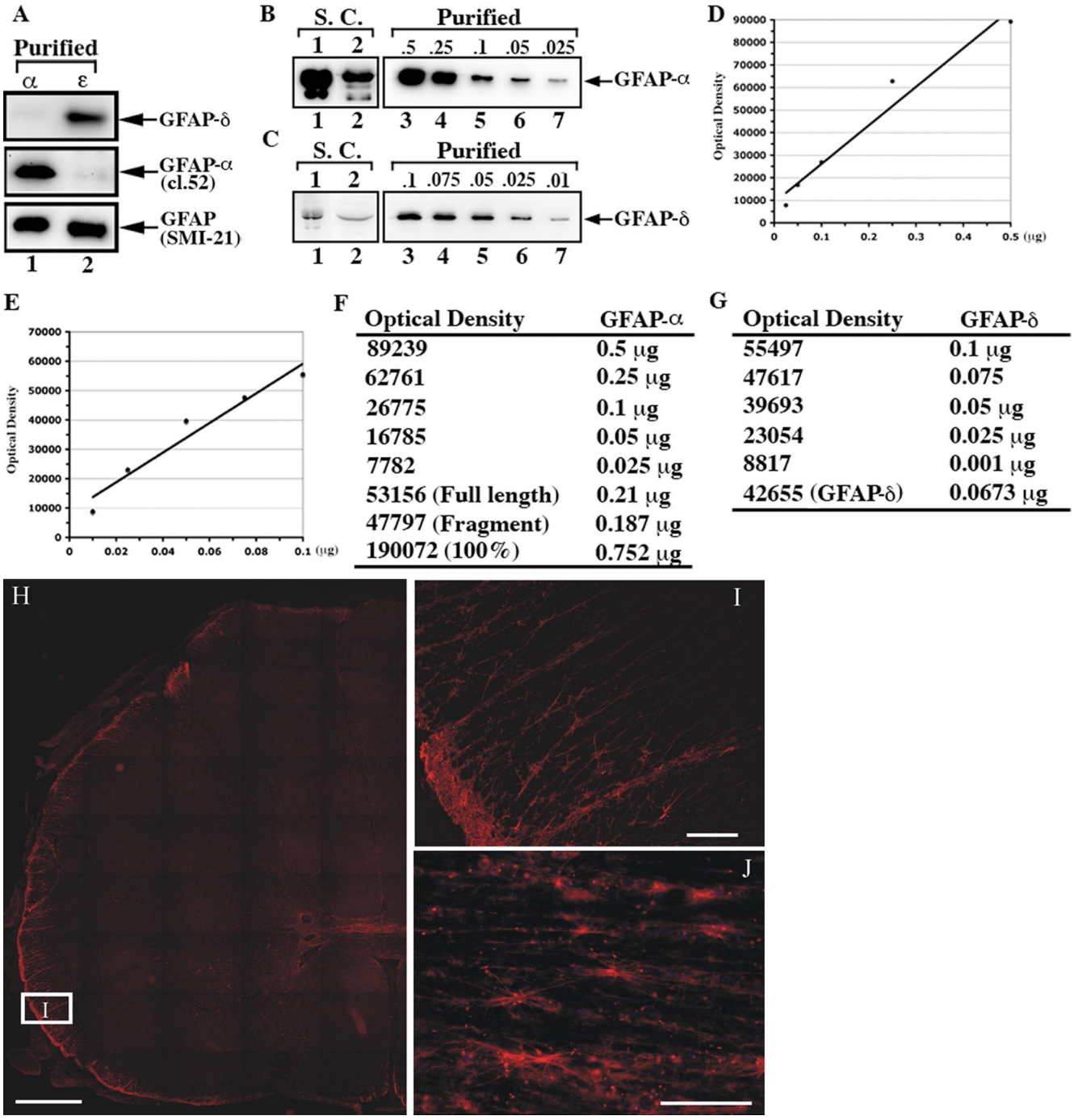

Figure 2. Characterization of the GFAP-δ antibody and demonstration of its presence in human spinal cord. The anti-human GFAP antibody, SMI-21, recognizes both GFAP-α and -δ (A, lanes 1 and 2, bottom panel). The anti-GFAP-α (clone-52) and anti-GFAP-δ antibodies (Roelofs *et al.*, 2005) recognized purified GFAP-α (A, lane 1, middle panel) and GFAP-δ (A, lane 2, top panel), respectively, confirming the specificity of these antibodies. The supernatant and pellet fractions prepared from two human spinal cord sample (S.C.) were analyzed by immunoblotting with antibodies to GFAP-α and -δ. Although very low levels of GFAP-α and -δ were detected in the supernatant fraction (data not shown), almost all immunopositive signals for GFAP-α and -δ were found in the pellet fractions (B and C, lanes, 1 and 2). The relative levels of GFAP-α to -δ were estimated by constructing standard curves (D and E) using dilutions of known concentrations of purified recombinant human GFAP-α and -δ (B and C, lanes 3–7). Quantification results are shown in F and G. Immunofluorescence localization of GFAP-δ in human spinal cord (H–J). (H and I) Horizontal sections; (J) a sagittal section of a cervical region human spinal cord sample. (I) A higher magnification of the boxed region in H (labeled I). H represents a tiled section of 45 individual fluorescent pictures showing half of a complete horizontal section of a human spinal cord. The patient was a 72-year-old woman. Bars, (H) 1 mm; (I and J) 100 μm.

using a harsh extraction buffer containing deoxycholate (Perng *et al.*, 2006). Under these extraction conditions, GFAP-α was almost completely extracted from both the untransfected (Figure 4F, lane 1, labeled S) and GFAP-α–transfected cells (Figure 4F, lane 3, labeled S). In contrast, GFAP-δ remained entirely in the pellet fraction of the

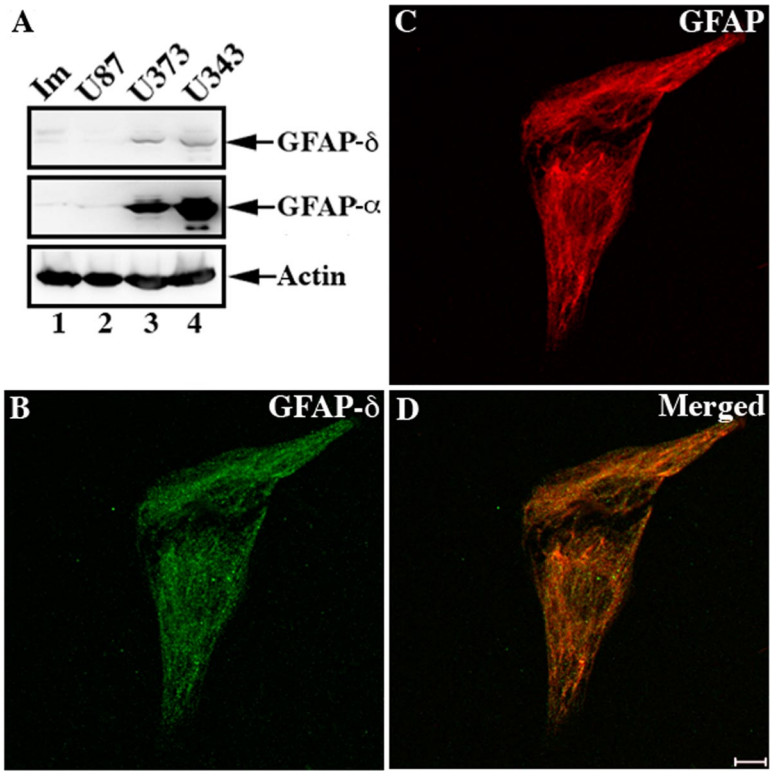

Figure 3. The presence of GFAP-δ in astrocytoma-derived cell lines. Immunoblotting of total cell lysates prepared from immortalized human astrocytes (Im) and human astrocytoma U87MG, U373MG, and U343MG cells were probed with antibodies to GFAP-α, -δ, and finally actin, which was used as a loading control (A). Although very low levels of endogenous GFAP-α and -δ were detected in Im (A, lane 1) and U87MG (A, lane 2) cells, both GFAP-α and -δ were expressed in U373MG (A, lane 3) and U343MG (A, lane 4) cells. The distribution of GFAP-δ in relation to whole GFAP networks in U343MG cells were visualized by double-label immunofluorescence microscopy using antibodies to GFAP-δ (B) and total GFAP (C). Notice the GFAP-δ signal was distributed alone the GFAP networks as shown in the merged image (D).

extracted cells transfected with GFAP-δ (Figure 4F, lane 6, labeled P). Quantification of Coomassie blue–stained gels showed the expression level of GFAP-δ in transfected U343MG cells was approximately equal to the endogenous total GFAP (Figure 4E, lane 6). These data suggest that, under normal physiological conditions, cells expressing low levels of GFAP-δ can successfully incorporate this into the endogenous GFAP networks. Increasing these levels of GFAP-δ by transient transfection disrupts the endogenous GFAP networks, leading to the formation of cytoplasmic GFAP-containing aggregates.

Addition of the eGFP Tag to the N-Terminus of GFAP Disrupts Assembly

These data suggest that assembly incompetence in vitro does not prevent inclusion into filament networks in living cells, providing that levels of this assembly-compromised form is at a permissible level relative to GFAP-α. The addition of GFP to the N-terminus of vimentin has been shown to be disruptive to filament assembly (Herrmann *et al.*, 2003) and yet this has been an effective tool to monitor vimentin dynamics in living cells (Ho *et al.*, 1998; Yoon *et al.*, 1998). We therefore decided to investigate the influence of eGFP upon GFAP assembly (Figure 5). The eGFP coding sequence was fused in-frame to the N-terminus of the GFAP-α and transfected into U343MG cells. Expression of eGFP-GFAP resulted in the formation of GFAP-enriched aggregates in ~80% of the transiently transfected cells (Figure 5, A and C). In some cells, however, expressed eGFP-GFAP was incorporated into the endogenous GFAP networks without obviously affecting its organization (Figure 5, D and E). Using standard in vitro assembly procedures, eGFP-GFAP failed to self-assemble into IFs or any IF-like structures (Figure 5F). Instead, it formed irregular filament-like material with beaded morphology that had a strong tendency to laterally associate into aggregates (Figure 5F).

The Alexander Disease Mutation R416W Incorporates in Filament Networks in U343MG Cells

Our previous studies had demonstrated that the disease-causing mutation R416W in GFAP seriously perturbed filament assembly both in vitro and in cultured cells (Perng *et al.*, 2006), but it also could be integrated into filament networks in astrocytes of affected individuals. This suggested to us that it was the relative level of R416W GFAP to total GFAP that determined whether the mutant would incorporate successfully into filament networks or induce filament aggregation. We therefore established a stable, inducible cell line to test this hypothesis.

Using the human astrocytoma U343MG cells with a Tet-Off gene expression system (Tsugu *et al.*, 2000), we selected a stable transfectant (U343-GFAP^{R416W}) that expresses R416W GFAP in response to doxycycline in a dose-dependent manner. When doxycycline is present in the cell culture medium, expression of R416W GFAP in U343-GFAP^{R416W} cells is inhibited, whereas in its absence R416W GFAP expression is induced in a controlled manner contrasting the uncontrolled overexpression achieved by transient expression which induces aggregate formation (Perng *et al.*, 2006). Cytoskeletal fractions prepared from uninduced (Figure 6A, lane 2) and induced U343-GFAP^{R416W} cells (Figure 6A, lane 1) were visualized by Coomassie blue staining, followed by immunoblotting analysis using the monoclonal anti-R416W GFAP antibody, 1A3, characterized previously (Perng *et al.*, 2006). A prominent band corresponding to the R416W GFAP was detected in induced cells as revealed by the 1A3 antibody (Figure 6B, lane 1), whereas this band was barely detectable in uninduced cells (Figure 6B, lane 2). The amount of R416W GFAP relative to the endogenous total GFAP was determined using purified recombinant human wild type (Figure 6A, lanes 3–6) and R416W GFAP (Figure 6B, lanes 3–6) as standards. It was estimated that the in-

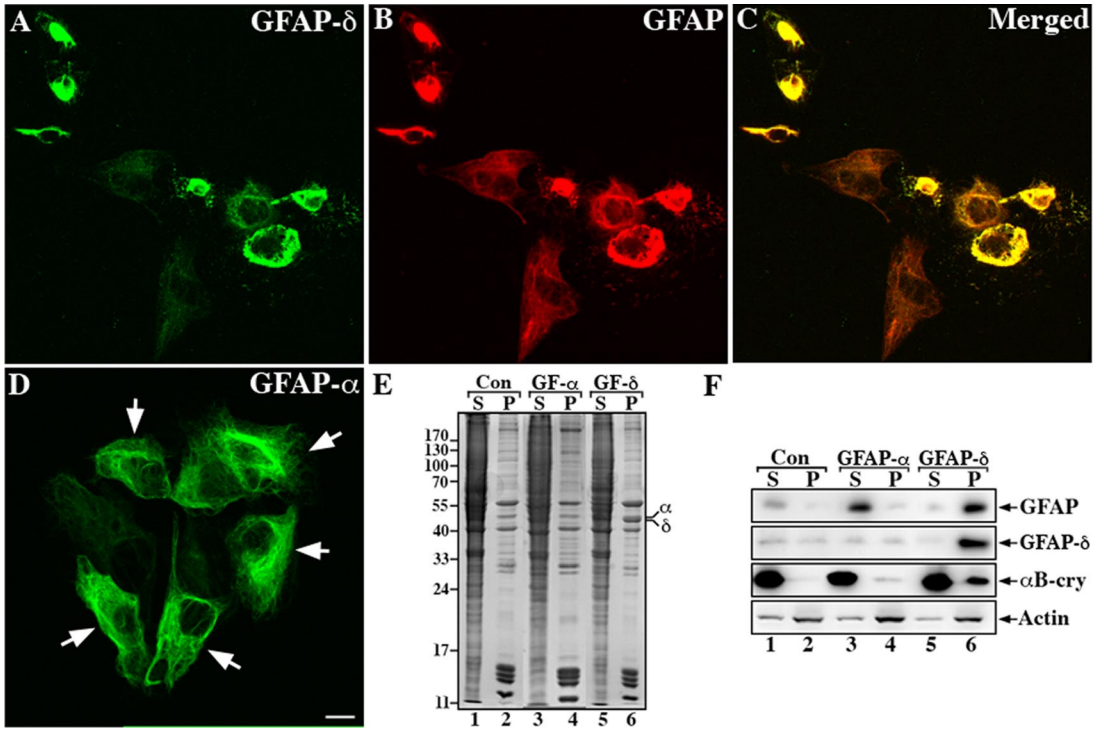

Figure 4. Overexpression of GFAP-δ resulted in the formation of cytoplasmic aggregates in U343MG cells. U343MG cells transiently transfected with either GFAP-δ (A–C) or GFAP-α (D) were fixed 48 h after transfection and visualized by double-label immunofluorescence microscopy using both anti-GFAP-δ (rabbit polyclonal; (Roelofs *et al.*, 2005) and a general anti-human GFAP antibodies (mouse monoclonal; GA5). The immunofluorescence for GFAP-δ is in the green channel (A), whereas the counterstaining for total GFAP is in the red channel (B). Merged images show the superimposition of both the green and red signals, and overlapping areas appearing yellow (C). Cells expressing GFAP-δ resulted in the formation of cytoplasmic aggregates that are immunopositive for both GFAP-δ (A) and total human GFAP (B). This is in contrast to cells transfected with GFAP-α, which mainly formed extended filament networks (D). Because there is no antibody available to distinguish transfected GFAP-α from the endogenous human GFAP, it was first necessary to titrate the anti-GFAP antibody to the point where the endogenous GFAP appeared as background staining on the untransfected cells. When GFAP levels are elevated by transient transfection, the signal becomes obvious above background (D, arrows). Bar, 10 μm. U343MG cells were either untransfected (lanes 1 and 2) or transfected with GFAP-α (lanes 3 and 4) or GFAP-δ (lanes 3 and 4). At 48 h after transfection, cells were extracted with harsh extraction buffer followed by centrifugation at 18,000 × *g* for 15 min at 4°C. The resulting supernatant (S) and pellet (P) fractions were separated by SDS-PAGE followed by Coomassie blue staining (E) or immunoblotting (F). Under these extraction conditions, the GFAP signal was detected predominantly in the supernatant fraction of untransfected (F, lane 1) and GFAP-α–transfected cells (F, lane 3), confirming the extraction efficiency. Immunoblotting with the anti-GFAP-δ antibody revealed that although the endogenous GFAP-δ was distributed in both soluble and insoluble fractions in both the untransfected (F, lanes 1 and 2) and GFAP-α–transfected cells (F, lanes 3 and 4), and ~90% of transfected GFAP-δ was found in the pellet fraction (F, lane 6). Equal loading for the various supernatant and pellet fractions were verified using an anti-actin antibody (F, lanes 1–6).

duced U343-GFAP^{R416W} cells expressed 10 times more R416W GFAP than uninduced cells (Figure 6B, cf. lane 1 and 2), but this expression level was still only ≤10% of total GFAP (Supplementary Figure S2). The expression level of R416W GFAP is therefore relatively low compared with the endogenous GFAP in U343-GFAP^{R416W} cells. Double-label immunofluorescence microscopy showed that the expression of R416W GFAP (Figure 6C) resulted in its incorporation into the endogenous GFAP networks (Figure 6D) in induced U343-GFAP^{R416W} cells (merged image; Figure 6E). When all these data are taken together, they suggest that GFAP filaments can tolerate the incorporation of a wide range of GFAP constructs that, by themselves, are assembly compromised.

Incorporation of Assembly-compromised GFAP-δ Changes the Interaction of the Filaments with Potential Associated Proteins

We considered that the incorporation of assembly-compromised forms of GFAP into the IF could change the way in which other cytoplasmic proteins would interact with the IFs. To test this hypothesis, we investigated the interaction of small HSP, αB-crystallin with GFAP as a protein that associates with GFAP filaments both in vitro (Perng *et al.*, 1999a,b) and in certain human pathologies involving IF aggregates (van den IJssel *et al.*, 1999). We used an established cosedimentation assay (Perng *et al.*, 1999b) to test whether αB-crystallin interacts differently with filaments formed by either GFAP-α or -δ or a mixture of GFAP-α and -δ (Figure 7). GFAP-α and -δ either on its own or in assembly mixtures assembled efficiently in vitro, with most of the GFAP (>92%) being found in the pellet fractions (Figure 7A, lanes 4, 6 and 8, labeled P). In the absence of GFAP, nearly all of the αB-crystallin remained soluble (Figure 7A, lane 1, labeled S), with only 8% of αB-crystallin being sedimented (Figure 7A, lane 2, labeled P). With the inclusion of GFAP-α, the proportion of pelletable αB-crystallin was marginally increased to 12% (Figure 7A, lane 4, labeled P). This is in stark contrast to mixing GFAP-δ with αB-crystallin, where 55% of αB-crystallin cosedimented with

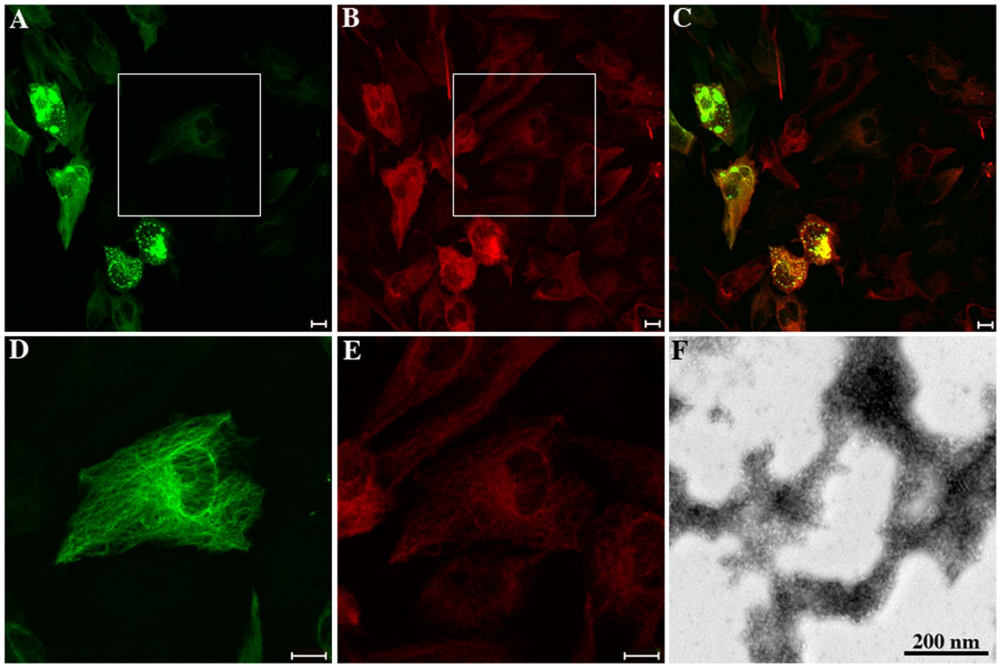

Figure 5. Transient expression of eGFP-GFAP perturbs IF network formation in cultured cells and disrupts filament assembly in vitro. eGFP-GFAP was transiently transfected into U343MG cells. At 48 h after transfection, cells were fixed, permeabilized, and counterstained with a standard GFAP antibody (SMI-21) to visualize the distribution of eGFP-GFAP (A) in relation to endogenous GFAP networks (B). Merged image shows that the expression of eGFP-GFAP resulted in aggregate formation in most of the transfected cells (C). Enlargements of the boxed areas in A and B showed eGFP-GFAP (D) integrate into the endogenous GFAP (E) and formed extended filament networks in some transfected cells. Bar, 10 μm. (F) Electron microscopic analysis of purified eGFP-GFAP chimeric protein confirmed that the eGFP tag fused at the N-terminus of GFAP interfere with normal assembly of GFAP in vitro (D). Bar, 200 nm.

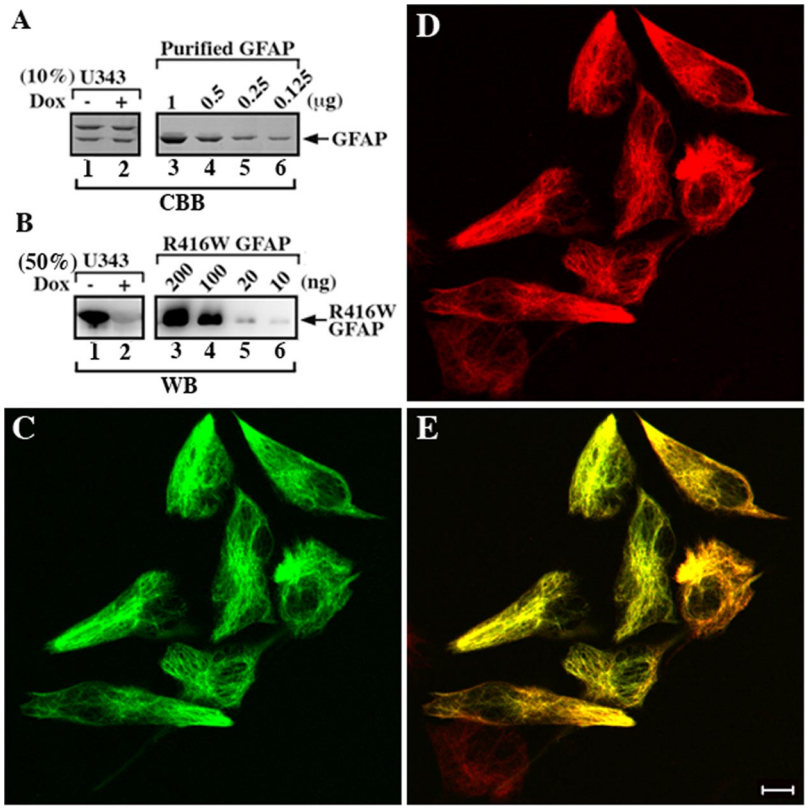

Figure 6. R416W GFAP can incorporate into the endogenous IF networks when expressed at a low level. Expression of R416W GFAP in U343-GFAP^{R416W} cells was induced by removal of doxycycline for 2 d. The cytoskeletal fractions prepared from induced (A and B, lane 1) and uninduced (A and B, lane 2) cells were separated by SDS-PAGE followed by Coomassie brilliant blue (CBB) staining (A) or immunoblotting (D). Representative gel shows that vimentin and GFAP are the major IF proteins in the cytoskeletal fractions (A, lanes 1 and 2). By immunoblotting, a prominent band corresponding to R416W GFAP was detected by 1A3 antibody in induced cells (B, lane 1), whereas it was barely detectable in uninduced cells (B, lane 2). The amount of total GFAP in the cytoskeletal fraction was determined by quantification of Coomassie blue–stained gel using known concentrations of purified recombinant human GFAP as standards (A, lanes 3–6). The level of R416W GFAP in induced U343-GFAP^{R416W} was determined against a standard curve generated by a serial dilution of known concentrations of bacterially expressed and purified R416W GFAP (B, lanes 3–6). The distribution of R416W GFAP in relation to the endogenous GFAP networks was visualized by double-label immunofluorescence microscopy using anti-R416W antibody (1A3) and standard anti-GFAP (3270) antibodies. When expressed in U343-GFAP^{R416W} cells, R416W GFAP (C) integrated into the endogenous GFAP networks (D). Merged image showed the region of colocalization between R416W GFAP and the endogenous GFAP appearing yellow (E). Bar, 10 μm.

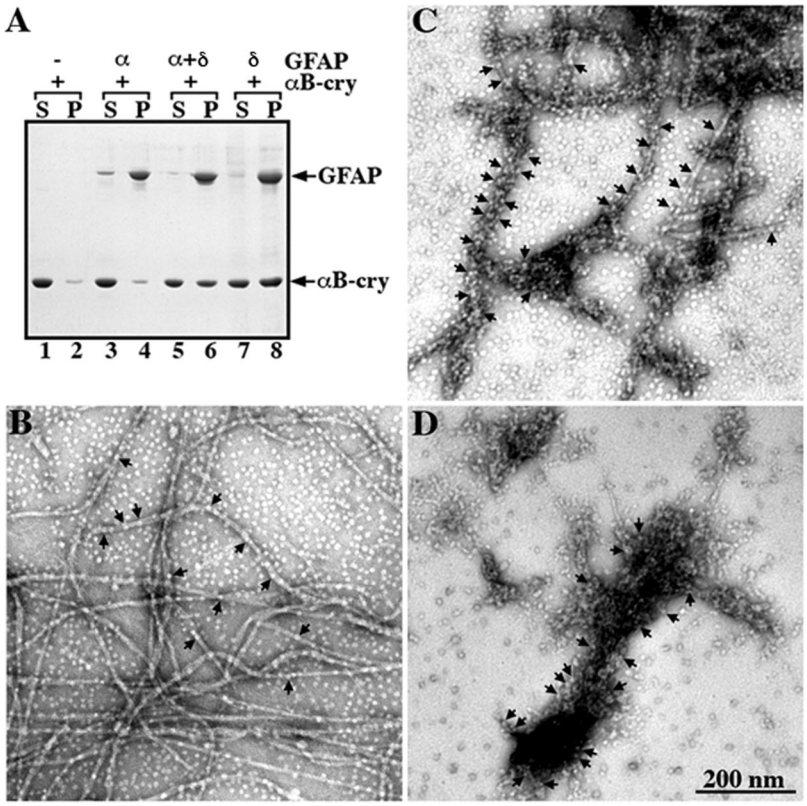

Figure 7. Binding of αB-crystallin to GFAP-δ containing filaments. GFAP-α and -δ, either individually or in a mixture of 90:10 of GFAP-α:-δ, were assembled in vitro in the presence of αB-crystallin at a molar ratio of 1:2 at 37°C for 1 h (A). The samples were subjected to high-speed centrifugation and the resulting supernatant (S) and pellet (P) fractions were analyzed by SDS-PAGE followed by Coomassie brilliant blue staining. A representative gel is shown, and the positions of GFAP and αB-crystallin are indicated. Under these assay conditions, αB-crystallin remained mostly in the supernatant (lane 1, labeled S) with only 8% being sedimented into the pellet fraction (lane 2, labeled P). When GFAP-α was included in the assay, only 12% of αB-crystallin cosedimented with GFAP-α into the pellet fraction (lane 4, labeled P). In contrast, αB-crystallin cosedimented more efficiently with GFAP-δ either as a mixture with GFAP-α or on its own. Increasing proportions of αB-crystallin (47 and 55%, respectively) were found in the pellet fractions (lanes 6 and 8, labeled P). After assembly, the binding of αB-crystallin to GFAP-α and -δ, either alone or as a mixture was visualized by electron microscopy. Under these assembly conditions, filaments formed by GFAP-α had some αB-crystallin particles attached (B, arrows). In contrast, the increased binding of αB-crystallin resulted in an extensive coating of GFAP-α/δ filaments (C, arrows). Coaggregation between GFAP-δ and αB-crystallin particles was seen (D, arrows). Bar, 200 nm.

GFAP-δ (Figure 7A, lane 8). Even the coassembly of GFAP-α with GFAP-δ in a 9:1 ratio in the presence of αB-crystallin resulted in the cosedimentation of 47% of the αB-crystallin (Figure 7A, lane 6).

These changes in the sedimentation behavior of αB-crystallin suggested increased binding to GFAP filaments. To investigate this possibility, samples were negatively stained and analyzed by electron microscopy (Figure 7, B–D). Although limited binding is seen to filaments assembled from GFAP-α (Figure 7B, arrows), the filaments comprising a 9:1 ratio of GFAP-α and -δ exhibited very obvious increase in αB-crystallin association (Figure 7C, arrows) as did the filamentous aggregates formed by GFAP-δ (Figure 7D, arrows). These data suggest that the inclusion of even a small proportion (10%) of GFAP-δ into GFAP-α filaments is sufficient to induce a significant change in their association with αB-crystallin in vitro.

To obtain biochemical evidence that the overexpression of GFAP-δ induces an increased association with αB-crystallin, U343MG cells were transiently transfected with GFAP-δ. Supernatant and pellet fractions were prepared using a mild extraction protocol, and immunoblotting analyses of these fractions revealed an increased proportion of αB-crystallin in the pellet fraction along with GFAP-δ (Figure 8A, lane 6). Similar results were obtained for cells transiently transfected with eGFP-GFAP (Figure 8A, lane 8) and R416W GFAP (Figure 8A, lane 10), but not for mock-transfected or GFAP-α transiently transfected cells (Figure 8A, lanes 2 and 4).

These data suggest that the overexpression of GFAP variants induce an increased association with αB-crystallin. HSP27 levels in the pellet fractions were only increased in the pellet fraction of R416W GFAP transfected cells (Figure 8A, lane 10), suggesting that the cellular response could be dependent on the specific GFAP variant that is being overexpressed. Therefore, we examined the activation status of the stress-activated protein kinase c-Jun amino-terminal kinase (SAPK/JNK) and found significant increases in p-JNK signal in the pellet fractions of cells expressing GFAP-δ (Figure 8A, lane 6), eGFP-GFAP (Figure 8A, lane 8), and R416W GFAP (Figure 8A, lane 10). Only low levels of p-JNK were detected in mock (Figure 8A, lanes 1 and 2) and GFAP-α–transfected cells (Figure 8A, lanes 3 and 4). It is however clear that the JNK phosphorylation response is not identical in all aspects for all samples with differences in the degree of p54/p46 phosphorylation for GFAP-δ, eGFP-GFAP, and R416W-GFAP (Figure 8, lanes, 6, 8, and 10, respectively). Double-label immunofluorescence microscopy demonstrated the colocalization of αB-crystallin (Figure 8C) and p-JNK (Figure 8E) with the GFAP-δ–containing aggregates (Figure 8, B and D). The data show that the overexpression of GFAP-δ induces the association of αB-crystallin and induces JNK phosphorylation.

DISCUSSION

GFAP-δ Is an Assembly-compromised Splice Variant of GFAP-α

Relatively few IF mRNAs produce distinct protein variants via alternative splicing, but those that do include Bfsp2 (CP49; Wallace *et al.*, 1998), lamin A/C (McKeon *et al.*, 1986; Furukawa and Hotta, 1993; Furukawa *et al.*, 1994; Machiels *et al.*, 1996), peripherin (Landon *et al.*, 1989; Robertson *et al.*, 2001; McLean *et al.*, 2008; Xiao *et al.*, 2008), and synemin (Xue *et al.*, 2004) as well as GFAP (Quinlan *et al.*, 2007). Little is known about the involvement of the different GFAP splice variants in either filament assembly or filament function. One novel splice variant, GFAP-δ, results in the replacement of C-terminal 42 amino acids of GFAP-α with a novel 41-amino acid sequence (Nielsen *et al.*, 2002; Quinlan *et al.*,

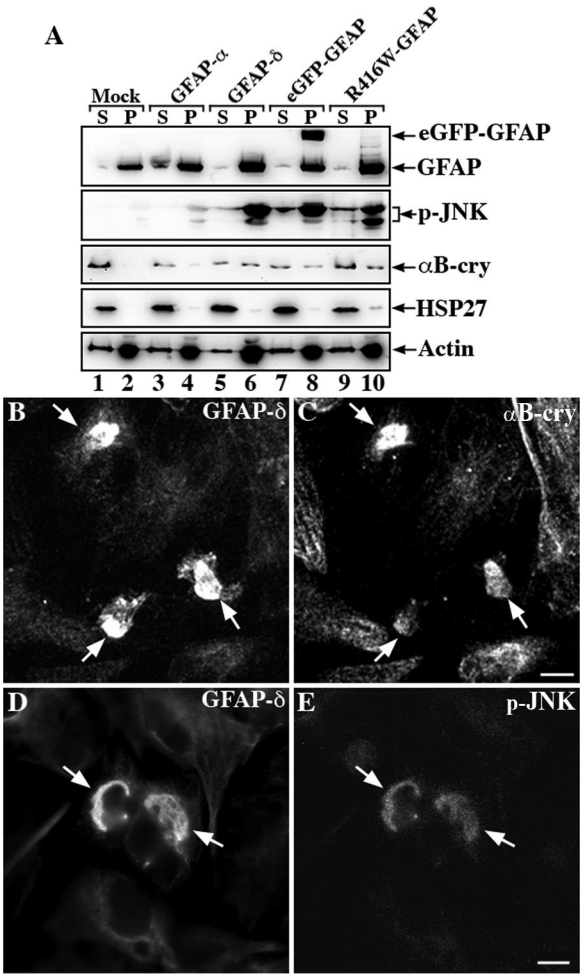

Figure 8. Analysis of GFAP variants expression in transfected U343MG cells. U343MG cells were transfected with indicated GFAP expression constructs. At 48 h after transfection, supernatant and pellet fractions were prepared from these cultures and were compared with mock-transfected cells. Using a mild extraction protocol, most of the endogenous GFAP was detected in the pellet fraction (A, lane 2, labeled P). Although GFAP-α was almost completely extracted into the supernatant fraction (A, lane 3, labeled S), GFAP-δ, eGFP-GFAP, and R416W GFAP remained in the pellet fractions (A, lanes 6, 8, and 10, labeled P). Immunoblots of the cell fractions were probed with antibodies to p-JNK, αB-crystallin, HSP27, and finally actin, which was used as a loading control. Notice that when cells were transfected with GFAP-δ, eGFP-GFAP, and R416W GFAP, a significant proportion of p-JNK and αB-crystallin but not HSP27 remained in the pellet fraction along with the GFAP variants (A, lanes 6, 8, and 10, labeled P). The distribution of αB-crystallin and p-JNK in relation to GFAP aggregates were examined by double-label immunofluorescence microscopy. U343MG cells transfected with GFAP-δ were stained with anti-GFAP-δ antibody (B and D) and costained with either αB-crystallin (C) or p-JNK (E). Notice that the GFAP-containing aggregates were positive for both αB-crystallin and p-JNK (B–E, arrows).

2007). Although initial studies suggested that the GFAP-δ tail inhibits homo-dimerization and filament formation as a result of direct interaction with the coiled-coil region of the rod domain (Nielsen and Jorgensen, 2004), its potential contribution to in vitro filament assembly has not been fully investigated.

Here we have shown that the new C-terminal tail domain of GFAP-δ affects its assembly properties in vitro. GFAP-δ failed to self-assemble into IFs, although combining this with GFAP-α restored filament assembly, providing the levels of GFAP-δ were low (10%). Our expression data for GFAP-δ in both the astrocyte cell lines and the spinal cord samples (Figures 2 and 3) also show that low levels (~10%) are consistent with incorporation into filament networks. Indeed, astrocytes in the subventricular zone clearly show a filamentous GFAP-immunostaining pattern (Roelofs *et al.*, 2005). Therefore, we conclude that GFAP-δ normally contributes to astrocyte function.

The fact that the expression level of GFAP-δ is not the same in all brain regions suggests a positive rather than a passive contribution to astrocyte cell function. A higher expression of GFAP-δ is clearly found in the subventricular zone of the human brain (Roelofs *et al.*, 2005), and we have shown staining of spinal cord astrocytes (Figure 2, H–J). In support of this conclusion, we show that altering GFAP-δ protein levels by transient transfection has deleterious effects (Figure 4), causing GFAP aggregate formation, the increased association of αB-crystallin and p-JNK (Figure 8), and the disruption of the endogenous GFAP networks (Figure 4).

GFAP Filaments Have a Natural Tolerance to Assembly-compromised Partners

A surprising point to emerge from our studies was the observation that filaments comprising GFAP-α were able to tolerate the incorporation of a small proportion (10–15%) of assembly-compromised protein. To explore the generality of this principle, we selected two quite different assembly-compromised GFAP constructs. The disease-causing mutant, R416W GFAP (Figure 6), and eGFP-GFAP (Figure 5) could be incorporated into the endogenous GFAP networks, providing the overexpression was kept relatively low. In the case of U343-GFAP^{R416W} the induced levels of R416W GFAP was ~10% of the endogenous GFAP levels, and this did not induce any noticeable network perturbation or filament aggregation.

A similar conclusion has been reached by other related studies. First, GFP-vimentin is assembly incompetent in vitro (Herrmann *et al.*, 2003), but can integrate into endogenous filament networks without any deleterious effects when overexpression levels are 20% of endogenous vimentin levels (Ho *et al.*, 1998). Second, the myopathy-causing mutation in desmin (R454W) was also capable of integration into the endogenous IF networks in cultured myoblasts containing a preexisting desmin IF network (Bar *et al.*, 2007). This mutation in desmin is directly equivalent to the R416W mutation in GFAP used in this study. The general question that then confronts us for GFAP-δ and the disease-causing mutations in GFAP is—Does the incorporation of such low levels of these assembly-compromised proteins affect the properties of the existing filament network?

Potential Functional Impact of GFAP Splice Variants: Modulation of GFAP Filament Properties?

We have previously demonstrated that αB-crystallin interacts with GFAP both in vitro and in cultured cells (Perng *et al.*, 1999a). In this study, our in vitro binding assays show that the inclusion of GFAP-δ, even to just 10% of the total GFAP, significantly increases the binding of αB-crystallin (Figure 7) as well as increasing the potential for GFAP filaments to aggregate (Figure 1F). We consider this as a proof of principle that the presence of GFAP-δ changes filament–filament associations and changes the association of other cytoplasmic proteins with the GFAP filaments, of which αB-crystallin is an example.

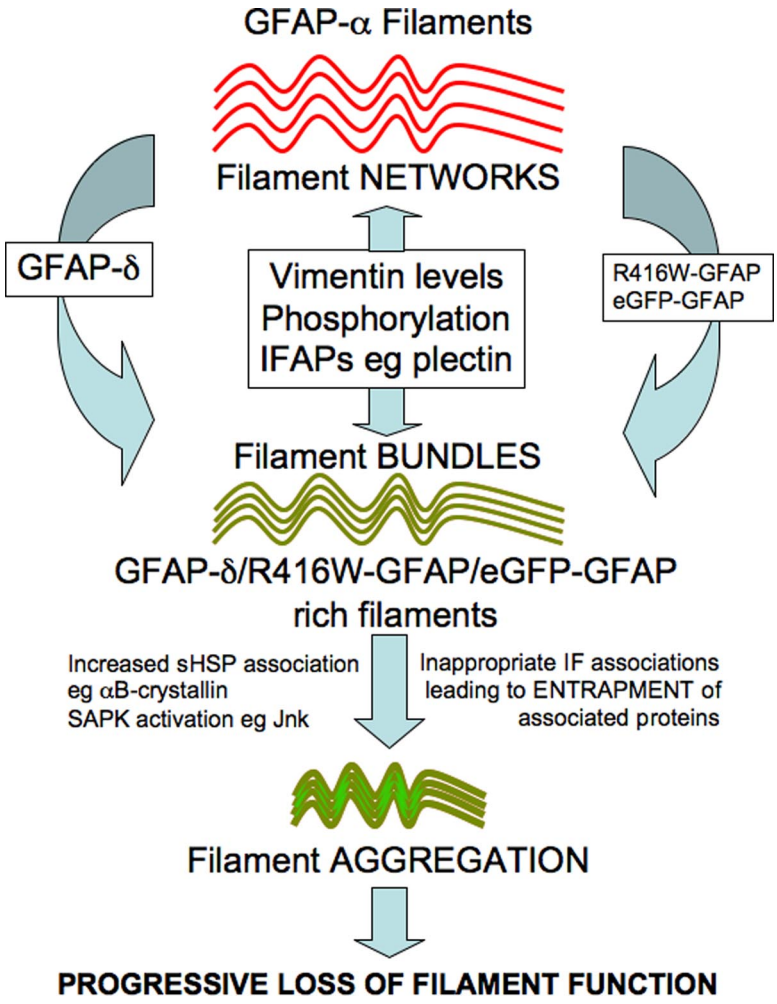

Figure 9. Model of GFAP filament modulation in cells. Our results from the tissue culture cells, U343MG and U373MG demonstrate that GFAP-δ coexists with GFAP-α in the GFAP filament networks in these cells. Disturbing the ratio of GFAP-δ:GFAP-α by the overexpression of GFAP-δ induced IF bundling and aggregation in transiently transfected cells. In vitro assembly studies demonstrate that filament–filament interactions and bundle formation are promoted by the presence of GFAP-δ, therefore suggesting that the balance of GFAP-δ in the filament networks can modulate interfilament associations in astrocytes. The presence of vimentin, as a GFAP assembly partner, is a proven mechanism to change interfilament spacing (Eliasson *et al.*, 1999). Although the mechanism(s) is unknown, IFAPs like plectin, a known IF cross-linker and the intermediate filament phosphorylation status are potential modulators of GFAP filament bundling (Tian *et al.*, 2006) and filament organization in cells (Yasui *et al.*, 1998). The transition from filament bundles to aggregates is also currently unknown, but is accompanied by the association of proteins like αB-crystallin (Perng *et al.*, 2006) and the phosphorylation of stress activated protein kinases like Jnk (Tang *et al.*, 2006). The imbalance in protein and filament associations can be induced, for instance by the increased proportion of assembly compromised and disease-causing GFAP mutants, leading to the entrapment and sequestration of associated proteins and the activation of stress kinase pathways (Tang *et al.*, 2006; Quinlan *et al.*, 2007).

The GFAP-δ has a completely different C-terminal tail domain and the consensus view is that the tail domains of type III IF proteins play an important role both in controlling filament width in vitro (Stewart *et al.*, 1989; Herrmann *et al.*, 1996) as well as in establishing proper IF networks in vivo (Eckelt *et al.*, 1992; McCormick *et al.*, 1993; Chen and Liem, 1994; Makarova *et al.*, 1994). Our data show that the presence of GFAP-δ changes the assembly and filament–filament interactions of the GFAP filaments (Figures 1 and 4). The tail domain of GFAP-δ could mediate specific interactions with a subset of cytoplasmic partners, such as presenilin (Nielsen *et al.*, 2002), but our data (Figure 7) show that its presence can increase αB-crystallin association and induce the phosphorylation of associated JNK with GFAP filaments. Therefore even though GFAP-δ levels are relatively low and the protein is assembly-compromised, it still is incorporated into the GFAP network and can potentially exhibit a measurable influence on GFAP filaments by changing filament–filament interactions, increase the association with αB-crystallin, and induce JNK phosphorylation.

There are several other ways to modulate GFAP filament functional properties in astrocytes (Figure 8). They include phosphorylation (reviewed in Sihag *et al.*, 2007), the incorporation of other IF proteins, such as vimentin and nestin (Herrmann and Aebi, 2000), and the association of IFAPs such as 14-3-3 (Satoh *et al.*, 2004; Li *et al.*, 2006) and αB-crystallin (Koyama and Goldman, 1999). Astrocyte activation increases GFAP-δ expression (Roelofs *et al.*, 2005) and induces 14-3-3 association with GFAP filaments (Li *et al.*, 2006). Therefore splice variant expression, in addition to posttranslational modification, coassembly partner, and the association of certain IFAPs are complimentary mechanisms to alter GFAP filament organization and filament properties in astrocytes (Figure 9). These mechanisms can also lead to increased filament–filament associations and aggregate formation, but this is usually in the context of disease for GFAP (Perng *et al.*, 2006; Tang *et al.*, 2006).

Splice Variants to Modulate IF Properties: An Emerging Pattern for Type III IF Proteins

These studies on GFAP-δ highlight an emerging pattern for the assembly of type III IFs in terms of the incorporation of other filament subunits to modulate IF function. For instance, nestin like GFAP-δ is also assembly-compromised in vitro, but it efficiently coassembles with vimentin (Steinert *et al.*, 1999) to regulate its assembly in cells via phosphorylation (Chou *et al.*, 2003) and to affect apoptotic cell signaling pathways (Sahlgren *et al.*, 2006). Desmin requires paranemin for network formation in cells (Schweitzer *et al.*, 2001). So both vimentin and desmin utilize other IF proteins to elicit changes in their filament properties, but peripherin and GFAP achieve a similar result by producing multiple splice variants from a single gene.

The parallels between the GFAP and peripherin genes with respect to multiple splice variants and disease-specific isoforms are striking. Both genes produce assembly-compromised splice variants (e.g., GFAP-γ/Per-45; Zelenika *et al.*,

1995; McLean *et al.*, 2008 and GFAP Δexon 6/Per28; Hol *et al.*, 2003; Xiao *et al.*, 2008). Several GFAP splice variants (Δ exon 6 and Δ164; Hol *et al.*, 2003) including GFAP-δ (Roelofs *et al.*, 2005) are also produced in response to disease. There is a major assembly competent GFAP isoform, GFAP-α (Reeves *et al.*, 1989; Brenner *et al.*, 1990), which is widely expressed, whereas, for instance, GFAP-δ appears more restricted in expression (Roelofs *et al.*, 2005). Similarly, the human peripherin gene produces one assembly-competent form (Per-58; Cui *et al.*, 1995) in addition to several assembly-compromised variants (e.g., Per-45, which requires Per-58 for integration into IFs in cells; McLean *et al.*, 2008). Per-45 exhibits a much broader expression in neuronal tissue and is the major isoform expressed in the brain, with Per-58 being the predominant species in the spinal cord and brain stem. Disease (amyotrophic lateral sclerosis) induces the peripherin splice variant, Per-28, which is also assembly-compromised and triggers filament aggregation when overexpressed (Xiao *et al.*, 2008). The combined data underline the importance of these splice variants in altering IF properties in different cellular contexts in both normal and disease situations.

ACKNOWLEDGMENTS

We thank Dr. M. Brenner (Department of Neurobiology, University of Alabama at Birmingham) Dr. J. T. Rutka (Division of Neurosurgery, University of Toronto) for generously providing U343MG cells and Dr. Jim Goldman (Department of Pathology, Columbia University) for immortalized human astrocytes. This work was supported by grants from National Institute of Neurological Disorders and Stroke (P01NS42803; R.A.Q.), International Foundation Alzheimer Research (ISAO 04511; E.H.), and the Dutch Brain Foundation (HsN 13F05.08; E.H.). The spinal cord tissue was obtained from The Netherlands Brain Bank, Netherlands Institute for Neuroscience, Amsterdam, The Netherlands. We would like to thank Mark Mizee for technical assistance.

REFERENCES

Balcarek, J. M., and Cowan, N. J. (1985). Structure of the mouse glial fibrillary acidic protein gene: implications for the evolution of the intermediate filament multigene family. Nucleic Acids Res. *13*, 5527–5543.

Bar, H. *et al.* (2007). Conspicuous involvement of desmin tail mutations in diverse cardiac and skeletal myopathies. Hum. Mutat. *28*, 374–386.

Bongcam-Rudloff, E., Nister, M., Betsholtz, C., Wang, J. L., Stenman, G., Huebner, K., Croce, C. M., and Westermark, B. (1991). Human glial fibrillary acidic protein: complementary DNA cloning, chromosome localization, and messenger RNA expression in human glioma cell lines of various phenotypes. Cancer Res. *51*, 1553–1560.

Brenner, M., Johnson, A. B., Boespflug-Tanguy, O., Rodriguez, D., Goldman, J. E., and Messing, A. (2001). Mutations in GFAP, encoding glial fibrillary acidic protein, are associated with Alexander disease. Nat. Genet. *27*, 117–120.

Brenner, M., Lampel, K., Nakatani, Y., Mill, J., Banner, C., Mearow, K., Dohadwala, M., Lipsky, R., and Freese, E. (1990). Characterization of human cDNA and genomic clones for glial fibrillary acidic protein. Brain Res. Mol. Brain Res. *7*, 277–286.

Chen, W. J., and Liem, R. K. (1994). The endless story of the glial fibrillary acidic protein. J. Cell Sci. *107*(Pt 8), 2299–2311.

Chou, Y. H., Khuon, S., Herrmann, H., and Goldman, R. D. (2003). Nestin promotes the phosphorylation-dependent disassembly of vimentin intermediate filaments during mitosis. Mol. Biol. Cell *14*, 1468–1478.

Condorelli, D. F., Nicoletti, V. G., Barresi, V., Caruso, A., Conticello, S., de Vellis, J., and Giuffrida Stella, A. M. (1994). Tissue-specific DNA methylation patterns of the rat glial fibrillary acidic protein gene. J. Neurosci. Res. *39*, 694–707.

Condorelli, D. F., Nicoletti, V. G., Barresi, V., Conticello, S. G., Caruso, A., Tendi, E. A., and Giuffrida Stella, A. M. (1999). Structural features of the rat GFAP gene and identification of a novel alternative transcript. J. Neurosci. Res. *56*, 219–228.

Coulombe, P. A., and Wong, P. (2004). Cytoplasmic intermediate filaments revealed as dynamic and multipurpose scaffolds. Nat. Cell Biol. *6*, 699–706.

Cui, C., Stambrook, P. J., and Parysek, L. M. (1995). Peripherin assembles into homopolymers in SW13 cells. J. Cell Sci. *108*(Pt 10), 3279–3284.

Ding, M., Eliasson, C., Betsholtz, C., Hamberger, A., and Pekny, M. (1998). Altered taurine release following hypotonic stress in astrocytes from mice deficient for GFAP and vimentin. Brain Res. Mol. Brain Res. *62*, 77–81.

Eckelt, A., Herrmann, H., and Franke, W. W. (1992). Assembly of a tail-less mutant of the intermediate filament protein, vimentin, in vitro and in vivo. Eur J. Cell Biol. *58*, 319–330.

Eliasson, C., Sahlgren, C., Berthold, C. H., Stakeberg, J., Celis, J. E., Betsholtz, C., Eriksson, J. E., and Pekny, M. (1999). Intermediate filament protein partnership in astrocytes. J. Biol. Chem. *274*, 23996–24006.

Furukawa, K., and Hotta, Y. (1993). cDNA cloning of a germ cell specific lamin B3 from mouse spermatocytes and analysis of its function by ectopic expression in somatic cells. EMBO J. *12*, 97–106.

Furukawa, K., Inagaki, H., and Hotta, Y. (1994). Identification and cloning of an mRNA coding for a germ cell-specific A-type lamin in mice. Exp. Cell Res. *212*, 426–430.

Gomi, H., Yokoyama, T., Fujimoto, K., Ikeda, T., Katoh, A., Itoh, T., and Itohara, S. (1995). Mice devoid of the glial fibrillary acidic protein develop normally and are susceptible to scrapie prions. Neuron *14*, 29–41.

Herrmann, H., and Aebi, U. (2000). Intermediate filaments and their associates: multi-talented structural elements specifying cytoarchitecture and cytodynamics. Curr. Opin. Cell Biol. *12*, 79–90.

Herrmann, H., Bar, H., Kreplak, L., Strelkov, S. V., and Aebi, U. (2007). Intermediate filaments: from cell architecture to nanomechanics. Nat. Rev. Mol. Cell Biol. *8*, 562–573.

Herrmann, H., Haner, M., Brettel, M., Muller, S. A., Goldie, K. N., Fedtke, B., Lustig, A., Franke, W. W., and Aebi, U. (1996). Structure and assembly properties of the intermediate filament protein vimentin: the role of its head, rod and tail domains. J. Mol. Biol. *264*, 933–953.

Herrmann, H., Hesse, M., Reichenzeller, M., Aebi, U., and Magin, T. M. (2003). Functional complexity of intermediate filament cytoskeletons: from structure to assembly to gene ablation. Int. Rev. Cytol. *223*, 83–175.

Ho, C. L., Martys, J. L., Mikhailov, A., Gundersen, G. G., and Liem, R. K. (1998). Novel features of intermediate filament dynamics revealed by green fluorescent protein chimeras. J. Cell Sci. *111*(Pt 13), 1767–1778.

Hol, E. M., Roelofs, R. F., Moraal, E., Sonnemans, M. A., Sluijs, J. A., Proper, E. A., de Graan, P. N., Fischer, D. F., and van Leeuwen, F. W. (2003). Neuronal expression of GFAP in patients with Alzheimer pathology and identification of novel GFAP splice forms. Mol. Psychiatr. *8*, 786–796.

King, R. J., Finley, J. R., Coffer, A. I., Millis, R. R., and Rubens, R. D. (1987). Characterization and biological relevance of a 29-kDa, oestrogen receptor-related protein. J. Steroid Biochem. *27*, 471–475.

Kinouchi, R., Takeda, M., Yang, L., Wilhelmsson, U., Lundkvist, A., Pekny, M., and Chen, D. F. (2003). Robust neural integration from retinal transplants in mice deficient in GFAP and vimentin. Nat. Neurosci. *6*, 863–868.

Koyama, Y., and Goldman, J. E. (1999). Formation of GFAP cytoplasmic inclusions in astrocytes and their disaggregation by alphaB-crystallin. Am. J. Pathol. *154*, 1563–1572.

Laemmli, U. (1970). Cleavage of structural proteins during the assembly of the head of bacteriophage T4. Nature *277*, 680–685.

Landon, F., Lemonnier, M., Benarous, R., Huc, C., Fiszman, M., Gros, F., and Portier, M. M. (1989). Multiple mRNAs encode peripherin, a neuronal intermediate filament protein. EMBO J. *8*, 1719–1726.

Lewis, S. A., Balcarek, J. M., Krek, V., Shelanski, M., and Cowan, N. J. (1984). Sequence of a cDNA clone encoding mouse glial fibrillary acidic protein: structural conservation of intermediate filaments. Proc. Natl. Acad. Sci. USA *81*, 2743–2746.

Li, H., Guo, Y., Teng, J., Ding, M., Yu, A. C., and Chen, J. (2006). 14-3-3gamma affects dynamics and integrity of glial filaments by binding to phosphorylated GFAP. J. Cell Sci. *119*, 4452–4461.

Machiels, B. M., Zorenc, A. H., Endert, J. M., Kuijpers, H. J., van Eys, G. J., Ramaekers, F. C., and Broers, J. L. (1996). An alternative splicing product of the lamin A/C gene lacks exon 10. J. Biol. Chem. *271*, 9249–9253.

Makarova, I., Carpenter, D., Khan, S., and Ip, W. (1994). A conserved region in the tail domain of vimentin is involved in its assembly into intermediate filaments. Cell Motil. Cytoskelet. *28*, 265–277.

McCall, M. A., Gregg, R. G., Behringer, R. R., Brenner, M., Delaney, C. L., Galbreath, E. J., Zhang, C. L., Pearce, R. A., Chiu, S. Y., and Messing, A. (1996). Targeted deletion in astrocyte intermediate filament (Gfap) alters neuronal physiology. Proc. Natl. Acad. Sci. USA *93*, 6361–6366.

McCormick, M. B., Kouklis, P., Syder, A., and Fuchs, E. (1993). The roles of the rod end and the tail in vimentin IF assembly and IF network formation. J. Cell Biol. *122*, 395–407.

McKeon, F. D., Kirschner, M. W., and Caput, D. (1986). Homologies in both primary and secondary structure between nuclear envelope and intermediate filament proteins. Nature *319*, 463–468.

McLean, J., Xiao, S., Miyazaki, K., and Robertson, J. (2008). A novel peripherin isoform generated by alternative translation is required for normal filament network formation. J. Neurochem. *104*, 1663–1673.

Mignot, C., Boespflug-Tanguy, O., Gelot, A., Dautigny, A., Pham-Dinh, D., and Rodriguez, D. (2004). Alexander disease: putative mechanisms of an astrocytic encephalopathy. Cell. Mol. Life Sci. *61*, 369–385.

Nicholl, I. D., and Quinlan, R. A. (1994). Chaperone activity of alpha-crystallins modulates intermediate filament assembly. EMBO J. *13*, 945–953.

Nielsen, A. L., Holm, I. E., Johansen, M., Bonven, B., Jorgensen, P., and Jorgensen, A. L. (2002). A new splice variant of glial fibrillary acidic protein, GFAP epsilon, interacts with the presenilin proteins. J. Biol. Chem. *277*, 29983–29991.

Nielsen, A. L., and Jorgensen, A. L. (2004). Self-assembly of the cytoskeletal glial fibrillary acidic protein is inhibited by an isoform-specific C terminus. J. Biol. Chem. *279*, 41537–41545.

Oshima, R. G. (2007). Intermediate filaments: a historical perspective. Exp. Cell Res. *313*, 1981–1994.

Pekny, M. (2001). Astrocytic intermediate filaments: lessons from GFAP and vimentin knock-out mice. Prog. Brain Res. *132*, 23–30.

Pekny, M., Johansson, C. B., Eliasson, C., Stakeberg, J., Wallen, A., Perlmann, T., Lendahl, U., Betsholtz, C., Berthold, C. H., and Frisen, J. (1999). Abnormal reaction to central nervous system injury in mice lacking glial fibrillary acidic protein and vimentin. J. Cell Biol. *145*, 503–514.

Pekny, M., Leveen, P., Pekna, M., Eliasson, C., Berthold, C. H., Westermark, B., and Betsholtz, C. (1995). Mice lacking glial fibrillary acidic protein display astrocytes devoid of intermediate filaments but develop and reproduce normally. EMBO J. *14*, 1590–1598.

Pekny, M., and Pekna, M. (2004). Astrocyte intermediate filaments in CNS pathologies and regeneration. J. Pathol. *204*, 428–437.

Perng, M. D., Cairns, L., van den IJssel, P., Prescott, A., Hutcheson, A. M., and Quinlan, R. A. (1999a). Intermediate filament interactions can be altered by HSP27 and alphaB-crystallin. J. Cell Sci. *112*(Pt 13), 2099–2112.

Perng, M. D., Muchowski, P. J., van den IJssel, P., Wu, G. J., Hutcheson, A. M., Clark, J. I., and Quinlan, R. A. (1999b). The cardiomyopathy and lens cataract mutation in alphaB-crystallin alters its protein structure, chaperone activity, and interaction with intermediate filaments in vitro. J. Biol. Chem. *274*, 33235–33243.

Perng, M. D., Su, M., Wen, S. F., Li, R., Gibbon, T., Prescott, A. R., Brenner, M., and Quinlan, R. A. (2006). The Alexander disease-causing glial fibrillary acidic protein mutant, R416W, accumulates into Rosenthal fibers by a pathway that involves filament aggregation and the association of alpha B-crystallin and HSP27. Am. J. Hum. Genet. *79*, 197–213.

Perng, M. D., Wen, S. F., van den IJssel, P., Prescott, A. R., and Quinlan, R. A. (2004). Desmin aggregate formation by R120G alphaB-crystallin is caused by altered filament interactions and is dependent upon network status in cells. Mol. Biol. Cell *15*, 2335–2346.

Quinlan, R. A., Brenner, M., Goldman, J. E., and Messing, A. (2007). GFAP and its role in Alexander disease. Exp. Cell Res. *313*, 2077–2087.

Quinlan, R. A., Moir, R. D., and Stewart, M. (1989). Expression in *Escherichia coli* of fragments of glial fibrillary acidic protein: characterization, assembly properties and paracrystal formation. J. Cell Sci. *93*(Pt 1), 71–83.

Quinlan, R. A., and Franke, W. W. (1983). Molecular interactions in intermediate-sized filaments revealed by chemical cross-linking. Heteropolymers of vimentin and glial filament protein in cultured human glioma cells. Eur. J. Biochem. *132*, 477–484.

Quinlan, R. A., and Franke, W. W. (1982). Heteropolymer filaments of vimentin and desmin in vascular smooth muscle tissue and cultured baby hamster kidney cells demonstrated by chemical crosslinking. Proc. Natl. Acad. Sci. USA *79*, 3452–3456.

Ralton, J. E., Lu, X., Hutcheson, A. M., and Quinlan, R. A. (1994). Identification of two N-terminal non-alpha-helical domain motifs important in the assembly of glial fibrillary acidic protein. J. Cell Sci. *107*(Pt 7), 1935–1948.

Reeves, S. A., Helman, L. J., Allison, A., and Israel, M. A. (1989). Molecular cloning and primary structure of human glial fibrillary acidic protein. Proc. Natl. Acad. Sci. USA *86*, 5178–5182.

Robertson, J., Beaulieu, J. M., Doroudchi, M. M., Durham, H. D., Julien, J. P., and Mushynski, W. E. (2001). Apoptotic death of neurons exhibiting peripherin aggregates is mediated by the proinflammatory cytokine tumor necrosis factor-alpha. J. Cell Biol. *155*, 217–226.

Roelofs, R. F., Fischer, D. F., Houtman, S. H., Sluijs, J. A., Van Haren, W., Van Leeuwen, F. W., and Hol, E. M. (2005). Adult human subventricular, subgranular, and subpial zones contain astrocytes with a specialized intermediate filament cytoskeleton. Glia *52*, 289–300.

Sahlgren, C. M., Pallari, H. M., He, T., Chou, Y. H., Goldman, R. D., and Eriksson, J. E. (2006). A nestin scaffold links Cdk5/p35 signaling to oxidant-induced cell death. EMBO J. *25*, 4808–4819.

Satoh, J., Yamamura, T., and Arima, K. (2004). The 14-3-3 protein epsilon isoform expressed in reactive astrocytes in demyelinating lesions of multiple sclerosis binds to vimentin and glial fibrillary acidic protein in cultured human astrocytes. Am. J. Pathol. *165*, 577–592.

Sawada, K., Agata, K., Yoshiki, A., and Eguchi, G. (1993). A set of anti-crystallin monoclonal antibodies for detecting lens specificities: beta-crystallin as a specific marker for detecting lentoidogenesis in cultures of chicken lens epithelial cells. Jpn. J. Ophthalmol. *37*, 355–368.

Schweitzer, S. C., Klymkowsky, M. W., Bellin, R. M., Robson, R. M., Capetanaki, Y., and Evans, R. M. (2001). Paranemin and the organization of desmin filament networks. J. Cell Sci. *114*, 1079–1089.

Sihag, R. K., Inagaki, M., Yamaguchi, T., Shea, T. B., and Pant, H. C. (2007). Role of phosphorylation on the structural dynamics and function of types III and IV intermediate filaments. Exp. Cell Res. *313*, 2098–2109.

Steinert, P. M., Chou, Y. H., Prahlad, V., Parry, D. A., Marekov, L. N., Wu, K. C., Jang, S. I., and Goldman, R. D. (1999). A high molecular weight intermediate filament-associated protein in BHK-21 cells is nestin, a type VI intermediate filament protein. Limited co-assembly in vitro to form heteropolymers with type III vimentin and type IV alpha-internexin. J. Biol. Chem. *274*, 9881–9890.

Stewart, M., Quinlan, R. A., and Moir, R. D. (1989). Molecular interactions in paracrystals of a fragment corresponding to the alpha-helical coiled-coil rod portion of glial fibrillary acidic protein: evidence for an antiparallel packing of molecules and polymorphism related to intermediate filament structure. J. Cell Biol. *109*, 225–234.

Sullivan, S. M., Lee, A., Bjorkman, S. T., Miller, S. M., Sullivan, R. K., Poronnik, P., Colditz, P. B., and Pow, D. V. (2007). Cytoskeletal anchoring of GLAST determines susceptibility to brain damage: an identified role for GFAP. J. Biol. Chem. *282*, 29414–29423.

Tang, G., Xu, Z., and Goldman, J. E. (2006). Synergistic effects of the SAPK/JNK and the proteasome pathway on glial fibrillary acidic protein (GFAP) accumulation in Alexander disease. J. Biol. Chem. *281*, 38634–38643.

Tian, R., Gregor, M., Wiche, G., and Goldman, J. E. (2006). Plectin regulates the organization of glial fibrillary acidic protein in Alexander disease. Am. J Pathol. *168*, 888–897.

Tsugu, A. *et al.* (2000). Expression of p57(KIP2) potently blocks the growth of human astrocytomas and induces cell senescence. Am J Pathol *157*, 919–932.

van den IJssel, P., Norman, D. G., and Quinlan, R. A. (1999). Molecular chaperones: small heat shock proteins in the limelight. Curr. Biol. *9*, R103–R105.

Wallace, P., Signer, E., Paton, I. R., Burt, D., and Quinlan, R. (1998). The chicken CP49 gene contains an extra exon compared to the human CP49 gene which identifies an important step in the evolution of the eye lens intermediate filament proteins. Gene *211*, 19–27.

Wilhelmsson, U. *et al.* (2004). Absence of glial fibrillary acidic protein and vimentin prevents hypertrophy of astrocytic processes and improves post-traumatic regeneration. J. Neurosci. *24*, 5016–5021.

Xiao, S., Tjostheim, S., Sanelli, T., McLean, J. R., Horne, P., Fan, Y., Ravits, J., Strong, M. J., and Robertson, J. (2008). An aggregate-inducing peripherin isoform generated through intron retention is upregulated in amyotrophic lateral sclerosis and associated with disease pathology. J. Neurosci. *28*, 1833–1840.

Xue, Z. G., Cheraud, Y., Brocheriou, V., Izmiryan, A., Titeux, M., Paulin, D., and Li, Z. (2004). The mouse synemin gene encodes three intermediate filament proteins generated by alternative exon usage and different open reading frames. Exp. Cell Res. *298*, 431–444.

Yasui, Y., Amano, M., Nagata, K., Inagaki, N., Nakamura, H., Saya, H., Kaibuchi, K., and Inagaki, M. (1998). Roles of Rho-associated kinase in cytokinesis; mutations in Rho-associated kinase phosphorylation sites impair cytokinetic segregation of glial filaments. J Cell Biol. *143*, 1249–1258.

Yoon, M., Moir, R. D., Prahlad, V., and Goldman, R. D. (1998). Motile properties of vimentin intermediate filament networks in living cells. J. Cell Biol. *143*, 147–157.

Zelenika, D., Grima, B., Brenner, M., and Pessac, B. (1995). A novel glial fibrillary acidic protein mRNA lacking exon 1. Brain Res. Mol. Brain Res. *30*, 251–258.